Available online at www.sciencedirect.com
ScienceDirect
Cement and Concrete Research 36 (2006) 1460–1466
Cement and Concrete Research

Petrography study of two siliceous limestones submitted to alkali-silica reaction

Y. Monnin *, P. Dégrugilliers, D. Bulteel, E. Garcia-Diaz

Département Génie Civil, Ecole Nationale Supérieure des Techniques Industrielles et des Mines de Douai, 941, Rue Charles Bourseul, B.P. 10838, F-59508 Douai, France

Received 24 August 2005; accepted 22 March 2006

Abstract

This study presents the contribution of petrography to the comprehension of the alkali-silica reaction mechanism applied to two siliceous limestones. A petrography study was made on the two aggregates before reaction to define their relative proportions and types of reactive silica and to observe their distribution in the microstructure. Then a model reactor, constituted by the reactive siliceous limestone aggregate, portlandite and NaOH, was used to measure the swelling due to reaction of the silica with alkalis and the free expansion of the aggregates. The volume evolution between both aggregates was very different and could be explained by the preliminary petrographic study. It appears that the swelling of the aggregates is conditioned by the microstructure of the carbonated matrix, the quantity and the distribution of the reactive silica.

Keywords: Alkali-silica reaction; Siliceous limestone; Swelling; Petrography

1. Introduction

This publication presents the contribution of petrography in the study of two siliceous limestone aggregates submitted to alkali-silica reaction (ASR).

A methodology to measure the degree of chemical reaction of ASR on a reactive flint aggregate was developed several years ago by Bulteel et al. [1]. This methodology, based on the French normalized test AFNOR P18-589 [2], had been extended here to a siliceous limestone aggregate [3].

Using this model concrete subsystem, Bulteel et al. [4] also observed an increase of the porosity within the aggregates and revealed their internal degradations. They put forward the appearance of amorphous zones by a petrographic study. They also demonstrated that the increase in the molar fraction of silanol sites was correlated with the penetration of cations into the aggregates.

In the present study, petrography allows us to identify potential reactive silica types in two siliceous limestone aggregates and to be identified their microstructure characterized before ASR. These observations permit a better understanding of the ASR mechanism for each aggregate.

Table 1
Mineralogy of the aggregates

Mineral	SL1	SL2
	Weight (%)	
Calcite	71.4	81.7
Illite	10.3	3.8
Silica	7.8	5.6
Dolomite	6.7	8.1
K-feldspar	2.0	0.5
Clinochlore	1.5	–
Pyrite	0.3	0.3
Sum	100	100

* Corresponding author.
E-mail address: monnin@ensm-douai.fr (Y. Monnin).

0008-8846/$ - see front matter © 2006 Elsevier Ltd. All rights reserved.
doi:10.1016/j.cemconres.2006.03.025

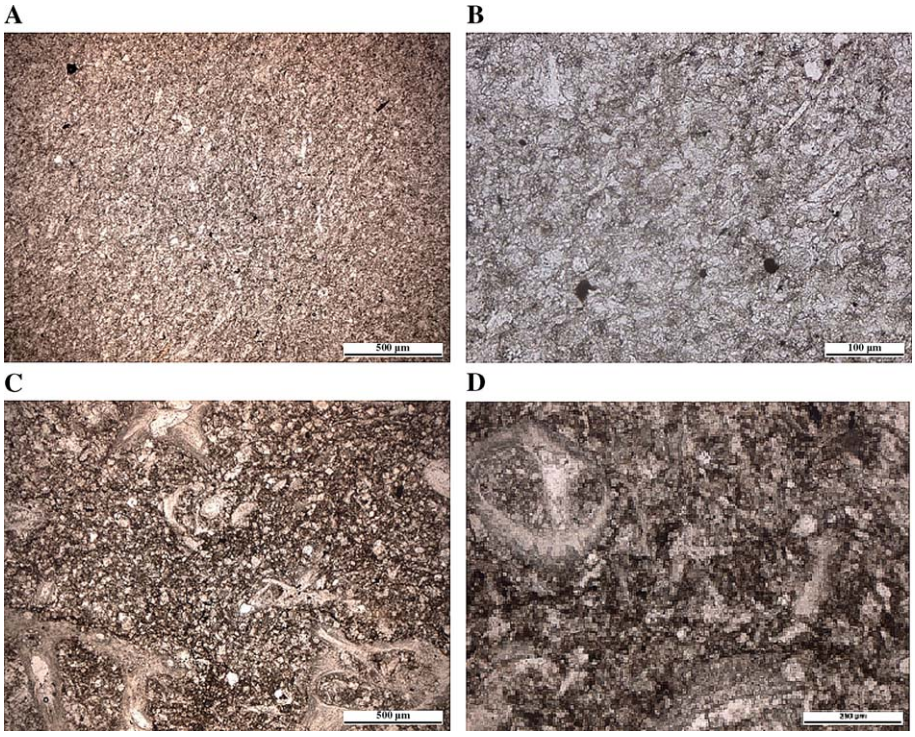

Fig. 1. Microstructure of the aggregates — A/B/C/D) Optical microscopy images with planed polars. Micrographs show the different microstructure of the aggregates at different scales. The microstructure of SL1 (A/B) is more homogenous than SL2 (C/D).

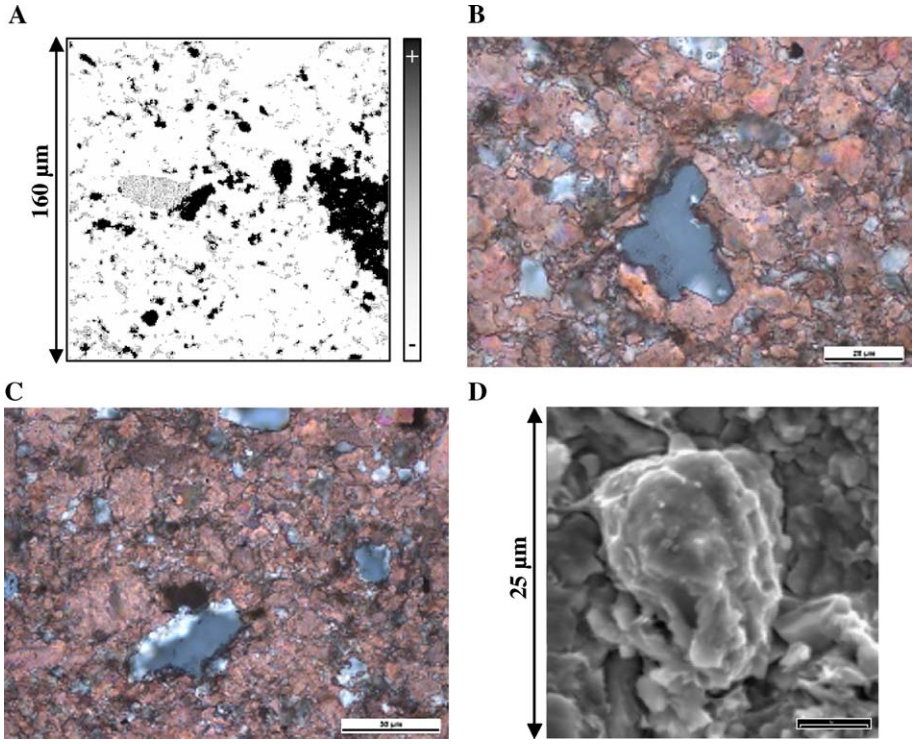

Fig. 2. Types of silica in SL1. A) Si-element map from SEM equipped with EDS probe revealing the homogenous repartition of silicon in the matrix. B/C) Optical microscopy micrographs with crossed polars treated with red alizarin shows the xenomorph silica without a well defined extinction. D) Micrograph from SEM of a xenomorph grain after light acid attack. (For interpretation of the references to colour in this figure legend, the reader is referred to the web version of this article.)

This article describes:

- the siliceous limestone aggregates and the petrographic study of the silica types;
- the chemical mechanism and the model reactor simulating the ASR;
- the measurements of the expansion of the silica and of the aggregates;
- the importance of these to the preliminary petrography.

2. Characterization of the aggregates

2.1. Origin of the siliceous limestone aggregates

The two siliceous limestone aggregates have been extracted from two different exploitation floors of a quarry from the North of Europe. Each floor is about 15 m height and is constituted by several geological beds. Consequently, the mineralogy of each mineral in one floor can fluctuate according to the different beds. In this study, the samples from every bed on each floor were treated as a single limestone type after bulk homogenisation. The size distribution of the aggregate was between 4 and 20 mm.

2.2. Mineralogical composition

The composition of the first siliceous limestone (Table 1) called "SL1" was characterized by Monnin et al. [3] for the main mineralogical constituents (wt.%>0.1). A quantitative analysis was carried out combining chemical measures and inorganic phases identified by X-ray diffraction, scanning electron microscope with EDS probe and optical microscopy. The same methodology was applied to the second siliceous limestone called "SL2" (Table 1).

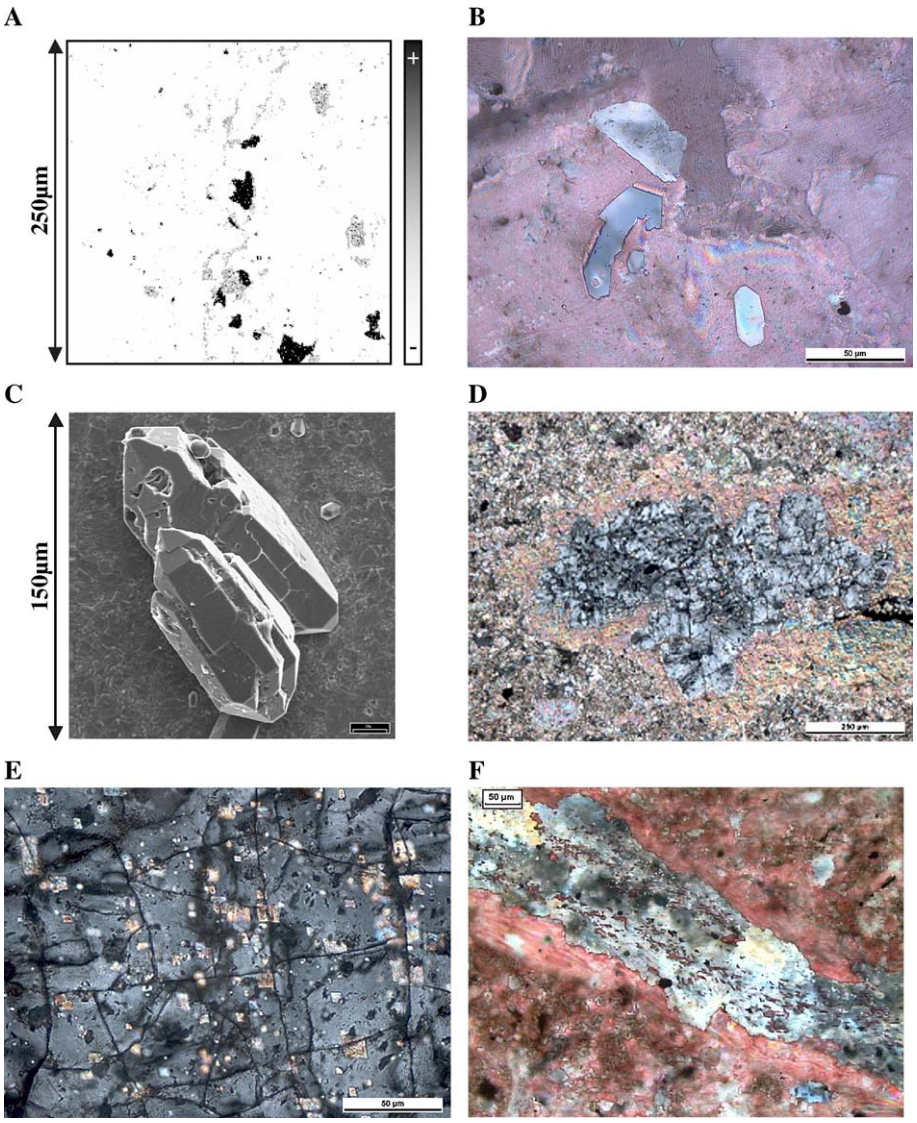

Fig. 3. Silica of SL2 — A) Si-element map from SEM equipped with EDS probe showing the heterogeneous distribution of silicon in the aggregate. B) Optical microscopy micrograph with crossed polars treated with red alizarin of automorph quartz. C) Micrograph from SEM of an automorph quartz with some structural flaws. D/E) Optical microscopy micrographs with crossed polars showing chalcedony with inclusions of dolomite. F) Optical microscopy micrograph with crossed polars treated with red alizarin of the lamellar silica. (For interpretation of the references to colour in this figure legend, the reader is referred to the web version of this article.)

Table 2
Potential reactivity of silica types and their proportion in both aggregates

Silica types	Reactivity potential	SL1	SL2
Automorph quartz	Weak	Not observed	Majority
Xenomorph silica	Strong	Majority	Not observed
Chalcedony	Strong	Not observed	Frequent
Microcrystalline quartz	Strong	Scarce	Scarce
Lamellar silica	Strong	Not observed	Scarce

According to the classification of Dunham [5], the siliceous limestone "SL1" is a mudstone. This is a micritic rock mainly consisting of calcite associated with a smaller quantity of dolomite (Fig. 1A and B). Several silicates were detected: phyllosilicates identified as illite and clinochlore. Illite is really more important and dispersed within the carbonated matrix. Potassium-feldspar and framboïdal pyrite were also present in fewer quantities. The types of silica in SL1 and SL2 will be described hereafter in a separate section on petrography.

The siliceous limestone "SL2" is classified as a packstone. This is a sparitic rock containing many bioclasts and massive crystallised calcite (Fig. 1C and D). In comparison, dolomite is more important than in SL1; illite and K-feldspar are presented in a fewer quantity than in SL1. Clinochlore was not observed.

On a smaller scale, optical microscopy revealed the relative homogeneity of the microstructure of SL1 (Fig. 1B) and by the contrasting, the more heterogeneous mineralogical assemblage of SL2 (Fig. 1D).

3. Petrography study of silica types

The petrography study was done after the homogenisation of the aggregates of each floor. Consequently, the proportion of silica types is somewhat variable in the studied aggregates. However, the optical characterization of a representative population allows us to estimate the relative proportion of each silica types in a floor.

The observations by optical microscopy have been carried out with thin sections in transmitted light with crossed polars. For a better visualization of the silica, calcite has been colorized in red with alizarin. A slight relief was generated by this treatment due to the acid solution. For the scanning electron microscopy (SEM), polished sections have been prepared by impregnation of the siliceous limestone aggregates by an epoxy resin. SEM was associated chemical analysis by energy dispersive spectroscopy (EDS) in order to quantify the chemical elements.

3.1. Silica types in SL1

The Si-element map, in Fig. 2A, reveals its homogenous distribution in the matrix. Free silica "SiO_2" is in dark; grey represents clays and K-feldspar. The main silica type is a xenomorph quartz (showing irregular outlines) with a grain size lower 50 μm. It is optically active without a well defined extinction (Fig. 2B and C). Another part of the silica is observed in the interstices of this mudstone associated with the clayey fraction. Light acid etching allows us to reveal this xenomorph silica within the carbonated matrix, the aspects are irregular (Fig. 2D). In this aggregate, the optical observation is very difficult due to the small size of the silica. Occasionally, microcrystalline quartz also observed in SL2 is detected.

3.2. Silica types in SL2

The Si-element map, in Fig. 3A, reveals the heterogeneity of the silicon distribution in the material. The free silica (in dark) is not much so dispersed as in SL1.

The main silica we observe in Fig. 3B, is an automorph quartz (showing crystal units with polyhedral outlines) which the limit size is of 150 μm. In transmitted light with crossed polars, these quartz have a well defined extinction without rolling. However, a light acid treatment reveals the presence of some structural flaws (Fig. 3C).

In many aggregates, fibrous chalcedony is frequently observed in a variable proportion and often enclosed in a massive calcite grains (Fig. 3D). Chalcedony generally contains many inclusions of dolomite (Fig. 3E). The last silica types observed occasionally are the microcrystalline quartz and a lamellar silica (Fig. 3F).

3.3. Reactivity of silica types

The petrographic study allowed us to determine the silica types constituting both siliceous limestone aggregates. In Table 2, the observed silica types are summarized and their relative proportion estimated from "majority" to "not observed". According to the ASR literature, the potential reactivity of each silica type is classified [6,7]. Consequently, SL1 is mainly constituted by the xenomorph silica which is

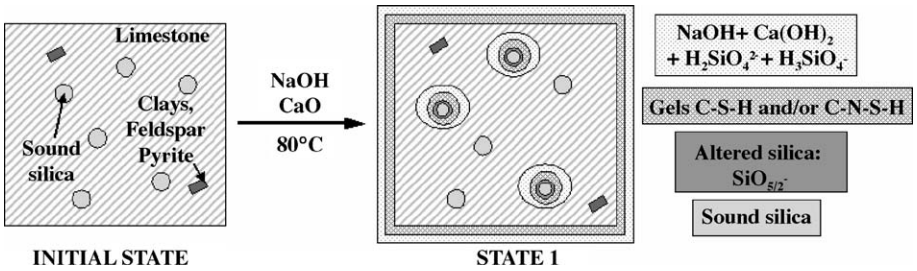

Fig. 4. Description of the model reactor method simulating ASR.

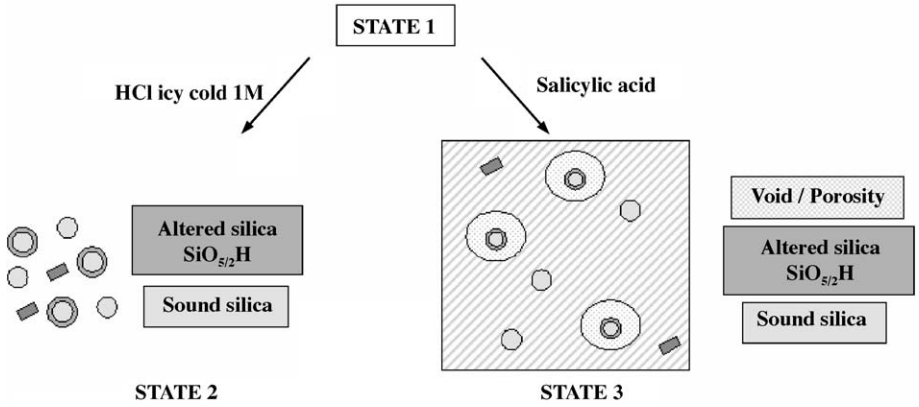

Fig. 5. Description of the different chemical treatments.

strongly reactive. On the other hand, SL2 is mainly constituted by automorph quartz which are not the most deleterious type. Only the frequently observed chalcedony seems to be the main source of reactivity.

4. Reactivity of the two siliceous limestone aggregates

4.1. Chemical mechanism of ASR

The ASR mechanism has described using different models [8–12] and can be written following two main steps:

➢ Formation of Q_3 tetrahedrons, due to destruction of siloxane bonds by hydroxyl ions attack:
Step 1:

$$2SiO_2 + OH^- \rightarrow SiO_{5/2}H + SiO_{5/2}^- \quad (1)$$

➢ Dissolution of silica, due to destruction of the other siloxane bonds of the Q_3 leading to Q_0 tetrahedrons:
Step 2:

$$SiO_{5/2}^- + OH^- + \frac{1}{2}H_2O \rightarrow H_2SiO_4^{2-} \quad (2)$$

Then the Q_0 tetrahedrons precipitate with alkalis in solution forming C–S–H and/or C–N–S–H gels.

4.2. Model reactor

The model reactor, which is a chemical sub-system constituted by portlandite, alkali base and reactive aggregate, has been developed. It allows the determination of the degree of the chemical reaction, volume variations of the silica and the aggregates at different reaction time [3]. This method is decomposed in two stages (Fig. 4):

Initial stage: A mix of 1 g of crushed aggregate and 0.5 g of portlandite is introduced in a closed stainless steel container. After 30 min preheating up to 80 °C, 10 ml of 0.79 M NaOH solution is added. The container is then autoclaved at 80 °C during different reaction times to accelerate ASR.

Stage 1: After the reaction, the aggregate is constituted with unaltered silica (Q_4) and with altered silica ($SiO_{5/2}Na$, $[SiO_{5/2}]_2Ca$ and $SiO_{5/2}H$).

4.3. Extraction of the silica and of the aggregates from state 1

The methodology, resumed Fig. 5, consists in two independent chemical treatments from state 1.

Stage 2: Selective acid treatment with 300 ml ice cold 1 M HCl solution allows us to dissolve ASR gels, portlandite, calcite, dolomite and protonate the ionised tetrahedrons $SiO_{5/2}Na$, $[SiO_{5/2}]_2Ca$ to $SiO_{5/2}H$. Finally, after filtration, drying and washing with an acetone–ether treatment, the solid residue is constituted by silica into Q_4 and Q_3 tetrahedrons and with clays, K-feldspar, pyrite and trace minerals.

Stage 3: The extraction of the aggregates is realised from state 1 thanks to a salicylic acid treatment in a methanol solution.

Table 3
Volume evolution of silica during ASR in both aggregates

Time (h)	Silica of SL1			Silica of SL2		
	$V^m_{absolute}(t)$ (mm^3/g)	$V^m_{porous}(t)$ (mm^3/g)	$V^m_{app}(t)$ (mm^3/g)	$V^m_{absolute}(t)$ (mm^3/g)	$V^m_{porous}(t)$ (mm^3/g)	$V^m_{app}(t)$ (mm^3/g)
0	374	38	412	380	25	405
8	373	45	418	382	29	411
13	375	46	421	385	29	414
16	374	47	422	383	32	415
20	376	47	423	383	33	416
24	376	48	425	381	34	416
37	381	49	430	388	36	424
48	383	59	442	387	35	422
72	386	60	446	390	39	429
120	393	67	460	387	44	431
168	399	69	468	399	49	447

Table 4
Volume evolution of the aggregates during ASR

Time (h)	Aggregate SL1			Aggregate SL2		
	$V^{m}_{absolute}(t)$ (mm^3/g)	$V^{m}_{porous}(t)$ (mm^3/g)	$V^{m}_{app}(t)$ (mm^3/g)	$V^{m}_{absolute}(t)$ (mm^3/g)	$V^{m}_{porous}(t)$ (mm^3/g)	$V^{m}_{app}(t)$ (mm^3/g)
0	369	7	376	369	10	378
8	368	12	380	366	11	377
13	365	19	383	368	10	378
16	370	15	385	364	14	378
20	369	18	387	364	14	378
24	368	19	388	368	11	379
37	366	27	394	369	12	379
48	368	27	395	369	13	382
72	369	26	395	370	13	383
120	371	26	398	372	12	384
168	369	30	399	371	13	384

4.4. Expansion of the silica and of the aggregates during ASR

4.4.1. Definition

Commonly, the expansion of a material is followed by the "apparent" mass volume and can be expressed as Eq. (3):

$$V^{m}_{app}(t) = V^{m}_{absolute}(t) + V^{m}_{porous}(t) \quad (3)$$

where $V^{m}_{absolute}(t)$ is the "absolute" mass volume occupied by the material, measured from Helium pycnometer on the crushed material.

$V^{m}_{absolute}(t)$ is the "porous" mass volume occupied by the material, measured without crushing on an accelerated surface area and porosimetry analyser based on the physical sorption of nitrogen following the B.J.H. method [13].

4.4.2. Expansions of the silica and of the aggregates

As described by Bulteel et al. [4] and Garcia-Diaz et al. [12], the competition between Step 1 and Step 2 of the mechanism inducing an expansion of the silica due to the accumulation of Q_3 tetrahedrons. The volume occupied by all reactive silica types in our siliceous limestone aggregates can be measured in Stage 2 (after HCl attack). In this study, the apparent mass volume variation after Stage 2 is considered as corresponding to the apparent mass volume variation of the silica types observed by petrography. Also, Table 3 gives the evolution of the different mass volumes of silica as a function of time.

The previous measurement methodology is applied on state 3 to follow the different volumes of the siliceous limestone aggregates during ASR (Table 4).

5. Results and discussion

Fig. 6 represents the swelling of both aggregates as a function of the expansion of the corresponding silica. The expansion of the aggregate SL1 is more important than the aggregate SL2 for an equivalent expansion of silica. After 7 days of reaction, in SL1 the swelling of the aggregate is about 20 mm^3/g for an expansion of the silica about 55 mm^3/g. The ratio of aggregate to silica expansion is less consequent in SL2 since the volume of the aggregates increases about 6 mm^3/g for an expansion about 42 mm^3/g of the silica. To explain these different evolutions, it is necessary to focus our attention on the reactive silica and on the microstructure of each aggregate.

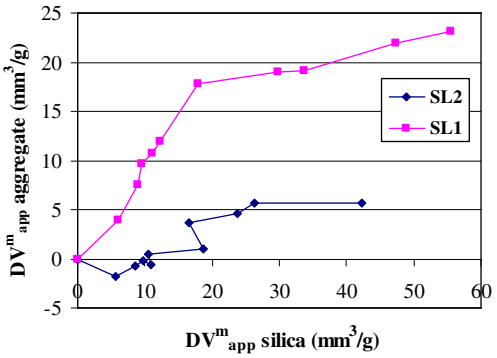

Fig. 6. Expansion of the aggregates as a function of the silica expansion.

The initial amount of silica introduced in the reactor is a little more important in SL1 than in SL2 due to the mineralogy of each aggregate. SL1 contains 7.8% of silica and SL2 only 5.6%. However, this explication seems to be too simplistic because it supposes the same silica reactivity in both aggregates. Thanks to the petrography study presented in paragraph 1, it has been observed that the potential reactivity is quite different between the two aggregates. SL1 is mainly constituted by a xenomorph silica very sensible to ASR. In the opposite, the major part of silica in SL2 is identified as automorph quartz fort which the potential reactivity is weak. Consequently, it seems to be logical that more expansion is measured in the case of the silica in SL1.

Nevertheless for a same expansion of silica, the response of the carbonated matrix is quite different. In SL1, an homogenous repartition of the reactive xenomorph silica (Fig. 2A, B and C) and a uniform carbonated matrix (Fig. 1A and B) lead to a higher expansion of the aggregate. In the opposite, SL2 which is constituted by a disordered matrix (Fig. 1C and D) containing variable proportions of massive chalcedony (Fig. 3D and E) is less expansive.

Consequently, the mineralogical arrangement of SL1 allows a higher expansion of the aggregates than in SL2. The heterogeneity of the matrix, the random repartition and the lower proportion of the reactive silica leads to chaotic and lower swelling in SL2.

6. Concluding remark

The petrographic study in the case of two siliceous limestone aggregates submitted to ASR is dual and summarized in Table 5.

Table 5
The main conclusions of the petrography

SL1	SL2
Homogenous repartition of reactive silica	Heterogeneous repartition of reactive silica
Higher proportion of reactive silica	Smaller proportion of reactive silica
Homogeneity of the microstructure	Heterogeneity of the microstructure
High expansion of the aggregate	Weak expansion of the aggregate

It allows the identification of reactive types of silica for both aggregates and also permits to the microstructure of each aggregate and the distribution of the reactive silica within the carbonated matrix to be characterized.

In the model reactor, the free expansion of the silica and the swelling of the aggregates have been measured at different reaction times. The siliceous limestone aggregate SL1 appears to be more expansive than SL2. Thanks to the conclusions of the petrography (Table 5), these comportments of both aggregates can be explained by their microstructure, the distribution and the reactivity of their silica contents, thanks to the petrographic study (Table 5).

This methodology based on the volume variations and on the petrography study seems to be a pertinent method to measure and determine the potential reactivity of a rock.

Acknowledgements

This study received a financial support from “Holcim Aggregates Belgium” and “Belgian Cements Company Ltd”.

References

[1] D. Bulteel, E. Garcia-Diaz, C. Vernet, H. Zanni, Alkali-silica reaction: a method to quantify the reaction degree, Cem. Concr. Res. 32 (2002) 1199–1206.
[2] AFNOR P18–589, Réactivité potentielle de type alcali-silice et alcali-silicate (test cinétique méthode chimique), 1991, p. 10.
[3] Y. Monnin, P. Dégrugilliers, D. Bulteel, E. Garcia-Diaz, Alkali-silica reaction: a method to quantify the reaction degrees in a siliceous limestone, Proceedings of the 12th ICAAR, Academic Publisher, Beijing, China, 2004, pp. 948–955.
[4] D. Bulteel, N. Rafaï, P. Degrugilliers, E. Garcia-Diaz, Petrography study on altered flint aggregate by alkali-silica reaction, Mater. Charact. 53 (2004) 141–154.
[5] R.J. Duhnam, Classification of carbonate rocks according to depositional texture, in: W.E. Ham (Ed.), Classification of Carbonate Rocks, Am. Assoc. Petrol. Geol. Mem., vol. 1, 1962, pp. 108–121.
[6] M.A.T.M. Broekmans, The crystallinity index of quartz by XRD, its susceptibility for ASR, and brief methodological review, Proceedings of the 12th ICAAR, Academic Publisher, Beijing, China, 2004, pp. 60–67.
[7] M.A.T.M. Broekmans, Structural properties of quartz and their potential role for ASR, Mater. Charact. 53 (2004) 129–140.
[8] L.S. Dent Glasser, N. Kataoka, The Chemistry of alkali-aggregate reaction, Proceedings of the 5th ICAAR, 1981, p. 7, Cape Town, South Africa.
[9] H. Wang, J.E. Gillott, Mechanisms of alkali-silica reaction and significance of calcium hydroxide, Cem. Concr. Res. 21 (1991) 647–654.
[10] A.B. Poole, Alkali-silica reactivity mechanisms of gel formation and expansion, Proceedings of the 9th ICAAR, London, England, Concr. Soc. Publ. CS104 1, 1992, pp. 782–789.
[11] R. Dron, F. Brivot, T. Chaussadent, Mécanisme de la réaction alcali-silice, Bull. Liaison Lab. Ponts Chaussées 214 (1998) 61–68.
[12] Garcia-Diaz, J. Riche, D. Bulteel, C. Vernet, Mechanism of damage for the alkali-silica reaction, Cem. Concr. Res. 36 (2006) 395–400.
[13] E.P. Barrett, L.G. Joyner, P.H. Halenda, J. Am. Chem. Soc. 73 (1951) 373.